Thermal diffusivity in mesophases: A systematic study in 4-4′-di-(*n*-alkoxy) azoxy benzenes

W. Urbach,[a] H. Hervet, and F. Rondelez

Physique de la Matière Condensée, Collège de France, 11 Place Marcelin-Berthelot, 75231 Paris Cédex 05, France

(Received 7 December 1981; accepted 1 June 1982)

We present a systematic study of thermal diffusivity in the nematic liquid crystalline phase of 4-4′-di-(*n*-alkoxy) azoxy benzenes and several other materials. The data allow to separate the respective contributions of the rigid central core and of the flexible aliphatic chains. For the component of the diffusivity tensor parallel to the long molecular axis, it is found that they differ by as much as a factor of 6 in favor of the core contribution. Combining the present observations with our earlier results, we are now able to draw general conclusions on the thermal diffusivity in a nematic and smetic A, B, and C phases. We have also developed two semiquantitative models based, one on a static network of distributed resistances, and the other on an extension of the Eyring kinetic model for the thermal conductivity of simple liquids. Only the dynamic model yields a satisfactory description of our data. The distance over which the thermal energy is not transferred instantaneously upon collision between two neighboring molecules is found to correspond to the aliphatic chain length (calculated for a freely rotating chain). Using this formalism, *a priori* calculations of the thermal diffusivities can be performed, to better than 20%, for any rodlike liquid crystalline material.

I. INTRODUCTION

Much less experimental work has been devoted to thermal conductivity than to the other transport properties of liquid crystalline (LC) materials, e.g., mass diffusion, viscosity, or sound velocity. This is due to the absence of a microscopic theory to describe thermal transport and also to the lack of a convenient experimental method applicable to these anisotropic mesophases. The only well-established result[1,2] is that the thermal conductivity of nematic phases is greater parallel than perpendicular to the mean direction of molecular alignment—$D_{\parallel} > D_{\perp}$. In that context, the introduction by Eichler *et al.*[3] of a novel optical technique to measure thermal properties in ordinary liquids has raised considerable interest.[4] The name of forced Rayleigh light scattering (FRS) has later been coined by Pohl and Irniger[5] to this elegant, contact-free method. In two earlier papers,[6] we have presented the first thermal measurements using FRS in the nematic and in the various smectic phases. These experimental data have indicated that the thermal conductivity anisotropy in LC is independent of the long range positional ordering of the center of mass of the molecules. It has, therefore, been suggested[6(b)] that the origin of the anisotropy is related to the elongated geometrical structure of the constituting molecules.

In order to thoroughly investigate this last point, we present here a systematic investigation of the thermal diffusivity in the series of 4-4′-di-(*n*-alkoxy) azoxybenzenes and in several other materials. The proportionality of the thermal diffusivity anisotropy $\Delta D = D_{\parallel} - D_{\perp}$ to the orientational order parameter S[7] is first checked. The present investigations allow then to separate the relative contributions of the molecular rigid core and of the flexible chains to the thermal conductivity. In a second part, two different microscopic models are described and their relevance to the anisotropic thermal conductivity in LC phases is critically discussed. Only the kinetic model provides a satisfactory description of our experimental data.

II. EXPERIMENTAL

The experimental setup has been described in details elsewhere.[8,9] The basic idea of FRS is to induce in the sample a spatially periodic fluctuation of temperature and to observe its subsequent relaxation by thermal diffusion.

In semitransparent samples, this transient thermal grating is produced by illuminating the sample with an optical interference pattern. A sinusoidal modulation is achieved by crossing two beams issued from the same Ar^+ laser under an angular separation ψ. For $\psi = 20$ mrad the resulting fringe spacing is $i = 25$ μm (Fig. 1).

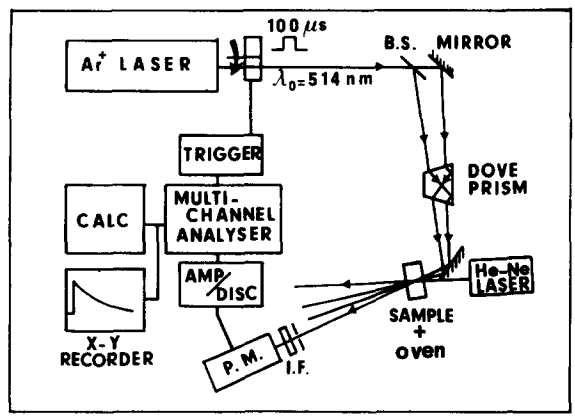

FIG. 1. Experimental setup. The argon laser (Spectra Physics model 165) is used to create the temperature pattern by light absorption in the sample at $\lambda_0 = 5\,145$ Å. The He–Ne laser (Spectra Physics model 133) is used for monitoring the time decay of the induced thermal grating. The Dove prism permits to rotate the fringe orientation relative to the sample axes. The phototube is a 56 TVP from Radiotechnique-Compelec. Its output is fed through a pulse amplifier to a multichannel analyzer BM 25 from Intertechnique used in the multiscaler mode. The calculator is a Hewlett–Packard 9825 and allows on-line treatment of the data.

[a] Permanent address: Lab. Biophysique (ERA 498) C. H. U. Cochin 24 Fb St-Jacques 75674 Paris Cèdex 14.

[b] Equipe de Recherche Associée au C.N.R.S. n° 542.

 0021-9606/83/085113-12$2.10

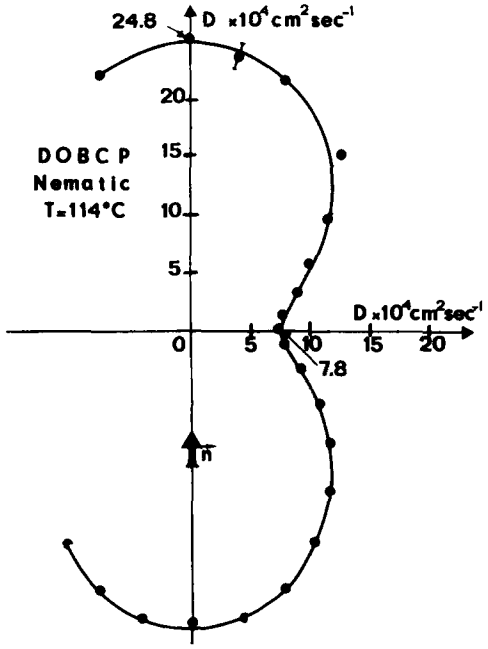

FIG. 2. Polar diagram of the thermal diffusivity coefficient in the nematic phase of di-(4-*n*-decyloxybenzal)-chloro-1-4-phenylene diamine at 114°C. The measurements have been made by rotating the fringe orientation relative to the sample optical axis n in a stepwise manner. The solid line is the best fit to the function $D(\theta)=D_{\parallel}\cos^2\theta+D_{\perp}\sin^2\theta$, where θ is the angle between n and the heat flow $D_{\parallel}=24.8\times10^{-4}$ cm^2 s^{-1}, $D_{\perp}=7.8\times10^{-4}$ cm^2 s^{-1}.

In our experiments, a mechanical chopper provided light pulses of 100 μs duration and the laser power was always lower than 200 mW. Suitable absorption of the writing laser beam in the sample was obtained by adding 5×10^{-4} g/g of methyl red (Merck, Darmstadt, Germany). In all cases, the temperature increase was less than 10 mK and the associated periodic change of refractive index was of the order of 10^{-5}–10^{-6}. This small change was nevertheless sufficient for the sample to

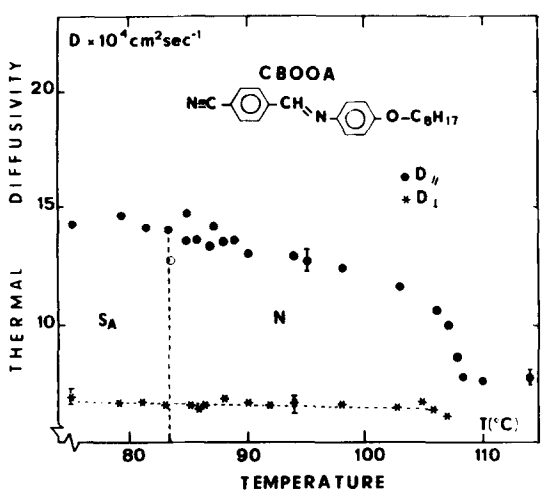

FIG. 3. Temperature dependence of the thermal diffusivity coefficients respectively parallel (●) and perpendicular (×) to the mean orientation axis in the nematic phase of *p*-cyanobenzili-dene-p-octyloxyaniline.

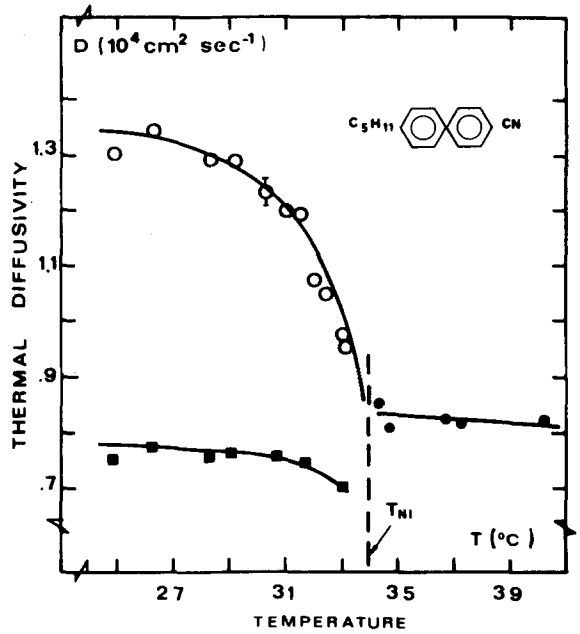

FIG. 4. Same as Fig. 2, but in the nematic phase of 4-*n*-pentyl-4-cyanobiphenyl.

behave as a transient optical (phase) grating and to diffract the beam of a 2 mW He–Ne probing laser. The characteristic decay time τ of the first order diffracted dot is directly related to the thermal diffusivity coefficient D by

$$\tau^{-1}=Dq^2\ ,$$

where $q=2\pi/i$ is the grating wave vector.

The signal was detected with a photomultiplier used in the photon counting mode and averaged over 100 measurements with a multichannel analyzer. Typical accuracy was 2% while overall reproducibility was 3%. The planar alignment in our 150–200 μm thick samples was obtained by an SiO deposition under oblique incidence[10] and checked optically by conoscopy and also by observation with collimated light between crossed polarizers. The samples were heated in a Mettler hot stage controlled to within 0.1 K and in which temperature gradients were less than 0.4 K/cm.

III. RESULTS

For all compounds studied, the measurements have been performed in the nematic phase exclusively. This does not represent a serious limitation since we have shown in Ref. 6(a) that the thermal diffusivity does not depend on the long-range positional ordering. On the other hand, it is shown in Fig. 2 that the thermal diffusivity strongly depends on the direction of the heat flow relative to the mean molecular alignment described by the director n. The temperature variation of the component of the thermal diffusivity tensor parallel $D_{\parallel}$ (perpendicular $D_{\perp}$) to n is displayed in Figs. 3–5 for *p*-cyanobenzilidene-*p*-octyloxyanilin (CBOOA for short), 4-*n*-pentyl-4-cyanobiphenyl (PCB) and seven compounds of the 4-4′-di-(*n*-alkoxy) azoxybenzene series (PAA1 to PAA9). In all cases, the variation is qualitatively the

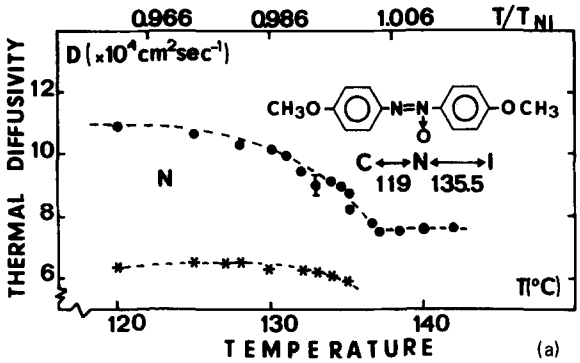

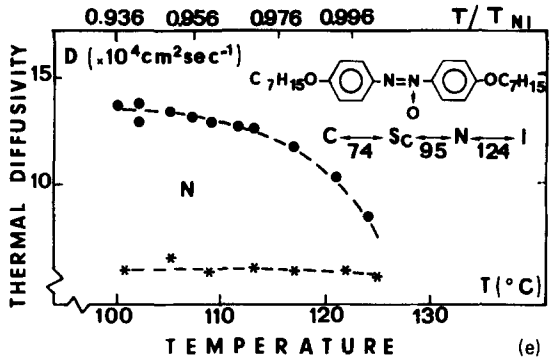

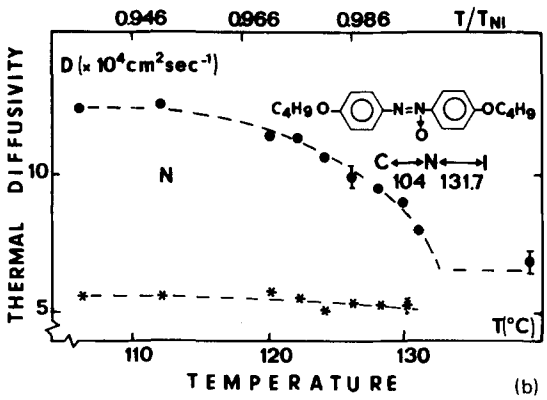

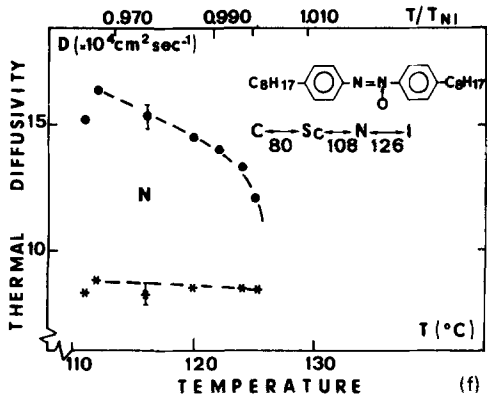

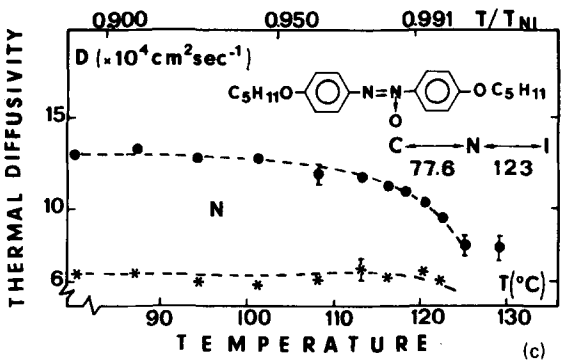

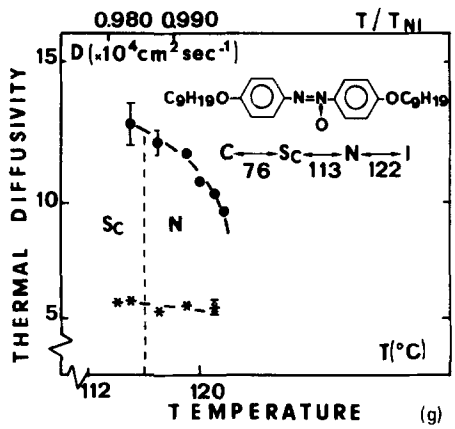

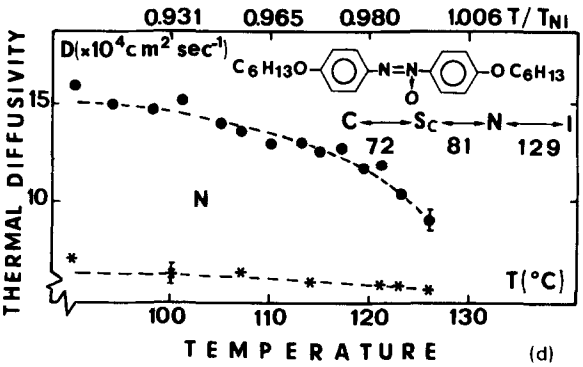

FIG. 5. (a)–(g) Same as Fig. 2, but in the nematic phase of the various homologs of the 4–4′-di-(*n*-alkoxy) azoxybenzene series.

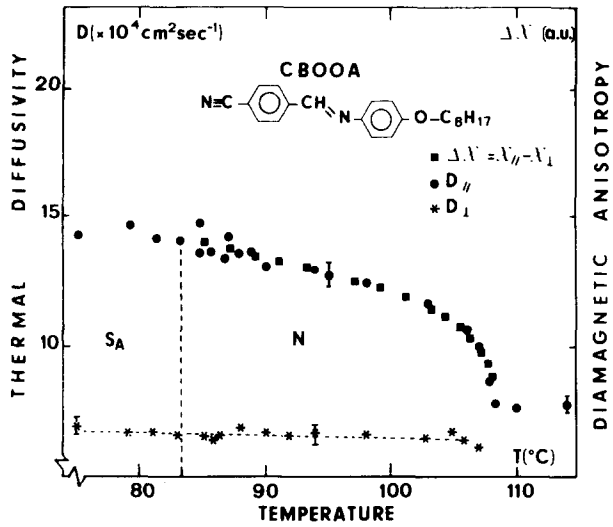

FIG. 6. Temperature dependences of the thermal diffusivity coefficients $D_{\parallel}$, $D_{\perp}$, (left axis) and of the diamagnetic ansiotropy $\Delta\chi$ (right axis) in the nematic phase of p-cyanobenzilidene-p-octyloxyaniline. The $\Delta\chi$ data have been taken from Ref. 11.

same. The ratio $D_{\parallel}/D_{\perp}$ is larger than one throughout the nematic temperature range and decreases continuously as the temperature T approaches the nematic–isotropic liquid transition temperature T_{NI}. In the isotropic phase, $D_{\parallel}/D_{\perp}$ is equal to unity. It should be remarked that no anomalous behavior is observed at the nematic to smectic C transition which occurs at low temperature for the higher members of the 4-4′-di-(n-alkoxy) azoxy benzene series [Figs. 5(a)–(g)]. This is fully consistent with our earlier observations at the nematic–smectic A transition.[6(a)]

IV. DISCUSSION

A. Temperature dependence of thermal diffusivities

It is interesting to compare the variations with temperature of the thermal diffusivity anisotropy $\Delta D = D_{\parallel} - D_{\perp}$ and of the orientational order parameter S.[7] By definition

$$S = \tfrac{1}{2}\langle 3\cos^2\theta - 1\rangle ,$$

where θ is the angle between the local optical axis $\mathbf{n}$ and the long axis of the rodlike molecules. S describes the degree of molecular alignment parallel to $\mathbf{n}$. $S \equiv 1$ for perfect alignment (corresponding to $\theta = 0$ or π), while $S = 0$ for random orientation (corresponding to $\langle\cos^2\theta\rangle = 1/3$).

It is generally agreed that S is proportional to the diamagnetic anisotropy $\Delta\chi = \chi_{\parallel} - \chi_{\perp}$.[7] The temperature dependence of this latter quantity has been measured by Hardouin *et al.*[11] in the nematic phase of CBOOA, which allows an easy comparison with our own measurements. This is done in Fig. 6 in which we have simultaneously plotted the temperature dependences of $D_{\parallel}$, $D_{\perp}$ and $\Delta\chi$. $D_{\parallel}(T)$ follows exactly $\Delta\chi$, while $D_{\perp}(T)$ stays approximately constant. Therefore, we can say that $\Delta D = D_{\parallel} - D_{\perp}$ and $\Delta\chi$ have identical temperature variations and that the thermal diffusivity anisotropy is directly proportional to the orientational order parameter S. To permit quantitative comparison between the various compounds, the measured thermal diffusivities, which are, in fact, thermal average values obtained for $S < 1$, must be normalized to a unique S value. The normalization procedure to $S = 1$ is shown in Appendix A. The standardized values D^s are written as

$$D^s_{\parallel} = \frac{D_{\parallel}(2+S) - 2D_{\perp}(1-S)}{3S}$$

and (1)

$$D^s_{\perp} = \frac{D_{\perp}(1+2S) - D_{\parallel}(1-S)}{3S} ,$$

where S is the order parameter value at the temperature of measurement T. Its exact temperature variation is not known for all the compounds studied here. However, if we consider that molecular interactions are temperature independent, the Maier–Saupe theory holds and S is, therefore, a universal function of T/T_{NI} which has been tabulated.[7] The standardized data calculated using Eq. (1) have been reported in Table I.

B. Comparison of the standardized data

1. *Perpendicular component of the diffusivity*

It is clear that $D^s_{\perp}$ does not vary dramatically with molecular length. For instance, the $D^s_{\perp}$ variation is less than 15% in the 4-4′-di-(n-alkoxy) benzene series even though the aliphatic chain length is multiplied by nine (if we except PAA-8 whose values seem abnormally high).

On the contrary, $D^s_{\perp}$ increases with the width of the central part of the molecule. This is best observed by comparing the $D^s_{\perp}$ values of DOBCP and PCB to the mean values of 4-4′-di-(n-alkoxy) azoxybenzenes and 4-n-pentyl-4 cyanoterphenyl (PCT), respectively. For the former compounds, the central part is quite wide. It comes from the fact that, in DOBCP, the three benzene rings are in *trans* configuration (Fig. 8) and that in PCB the molecules form dimers, the width of which is 1.4 times larger than the PCT single molecular width[12] (there is no evidence of dimer formation for PCT molecules). This explains why the $D^s_{\perp}$ value of 7.2×10^{-4} cm^2 s^{-1} for DOBCP is 50% larger than those of 4-4′-di-(n-alkoxy) azoxybenzenes and why the $D^s_{\perp}$ value for PCB is 40% larger than that of the PCT. In the first approximation, $D^s_{\perp}$ is thus observed to be proportional to the molecular width.

2. *Parallel component of the diffusivity tensor*

a. Dependence on aliphatic chain length L_a. We have plotted in Fig. 7 the dependence of $D^s_{\parallel}$ versus the number N of carbons atoms in the aliphatic chain of 4-4′-di-(n-alkoxy) azoxybenzenes. The variation is approximately linear and the data can be fitted to an empirical function

$$D^s_{\parallel}(N) = A + BN \qquad (2)$$

with $A = (12.8 \pm 1)\times10^{-4}$ cm^2 s^{-1} and $B = (0.54 \pm 0.2)\times10^{-4}$ cm^2 s^{-1} (C–C bond)$^{-1}$.

TABLE I. Thermal diffusivity results for the various liquid crystalline compounds investigated. The acronyms names are detailed below. M is the molar mass, T is the temperature of measurement, T_{NI} is the measured temperature of transition between the nematic and isotropic phases, S is the order parameter value at T, $D_{\parallel}$ and $D_{\perp}$ are the thermal diffusivity coefficients measured at T. $D_{\parallel}^{s}$ and $D_{\perp}^{s}$ are the diffusivity data normalized to $S=1$. $d_{\parallel}$ is the calculated length of the low thermally conducting regions as derived from the $D_{\parallel}^{s}$ and $D_{\perp}^{s}$ values using Eqs. (7) and (8) of the resistance model. L is the molecular length with the chains in all trans configurations. D_0 is derived from $D_{\parallel}^{s}$ using Eqs. (7) and the calculated $d_{\parallel}$ value. The computation of $d_{\parallel}$ and D_0 has been done with $a=5$ Å, $R=2.08$ Å, and $\alpha=1.43$. PAA_1 to PAA_9 stands for 4–4′-di(-p-alkoxyl) azoxy benzenes with the number of carbon atoms in the aliphatic chain ranging from 1–9. MBBA is for p-methoxy benzilidene-d-n-butyl aniline, BBOA is for p-butoxy benzilidene-p-n-octyl aniline, CBBOA p-eyanobenzilidene-p-octyl-oxyaniline, PCB 4-n-pentyl-4-cyanobiphenyl, PCT 4-n-pentyl-4-cyanoterphenyl, DOBCP di-(4-n-decyloxybenzal)-2-chloro-1-4-phenylene diamine.

Name	M g	T_{mes} °C	T_{NI} °C	T/T_{NI}	S	$D_{\parallel}$	$D_{\perp}$	$D_{\parallel}^{s}$	$D_{\perp}^{s}$	$d_{\parallel}$ Å	L Å	D_0
							10^{-4} cm^2 s^{-1}					10^{-4} cm^2 s^{-1}
PAA1	258	121.6	135.0	0.967	0.57	11.0	6.5	13.3	5.3	1.4	19.3	1.8
PAA4	342	117.6	131.7	0.965	0.57	12.0	5.5	15.3	3.8	1.2	26.8	1.3
PAA5	370	110.0	123.0	0.967	0.57	12.0	6.0	15.0	4.5	1.6	29.3	1.5
PAA6	398	113.6	129.0	0.962	0.57	13.0	6.0	16.5	4.2	1.5	31.8	1.4
PAA7	426	111.6	124.0	0.969	0.56	12.8	6.0	16.3	4.2	1.6	34.3	1.4
PAA8	454	116.0	126.0	0.975	0.54	15.4	8.6	19.2	6.6	2.3	36.8	2.2
PAA9	482	117.0	122.0	0.987	0.50	12.3	6.5	16.2	4.6	2.0	39.3	1.5
MBBA	267	34.0	45.0	0.965	0.57	13.3	7.5	16.2	6.0	1.4	20.6	2.0
BBOA	365	70.0	79.0	0.974	0.54	11.9	5.5	15.5	3.7	1.3	30.6	1.2
CBOOA	334	88.0	108.0	0.948	0.60	13.5	6.6	16.6	5.0	1.5	27.8	1.7
PCB	249	25.0	34.0	0.971	0.55	12.5	7.9	15.0	6.6	1.7	20.3	2.2
PCT	325	163.0	229.0	0.869	0.70	13.6	5.9	15.8	4.8	1.4	24.9	1.6
DOBCP	631	114.0	165.5	0.881	0.90	24.8	7.8	26.0	7.2	2.5	49.0	2.4

Adding one methyl group to the aliphatic chain corresponds to a length increase of 1.25 Å (projected onto the long molecular axis). Taking into account the fact that the compounds of the 4-4′-di-(n-alkoxy) azoxybenzene series are symmetric molecules, Eq. (2) can be converted to a mean diffusivity increase per unit length:

$$\Delta D_{\parallel}^{s}/\Delta L_a = (0.2 \pm 0.08) \times 10^{-4} \text{ cm}^2 \text{ s}^{-1} \text{ Å}^{-1} . \quad (3)$$

b. Dependence on core length L_c. For all members of the 4-4′-di-(n-alkoxy) azoxybenzenes, the core length is the same, $L_c \simeq 13$ Å. We can first estimate its contribution (per unit length) to the diffusivity from the A value in Eq. (2)

$$\Delta D_{\parallel}^{s}/\Delta L_c \simeq (1.0 \pm 0.1) 10^{-4} \text{ cm}^2 \text{ s}^{-1} \text{ Å}^{-1} . \quad (4)$$

The $D_{\parallel}^{s}$ dependence on L_c can also be deduced by comparing the $D_{\parallel}^{s}$ value measured for DOBCP and that calculated for 4-4′-di-n-decyloxy azoxybenzene using Eq. (2) with $N=10$. Indeed, both compounds have the same number of bonds in the aliphatic flexible chains and they only differ by the addition of one extra chloro-substituted phenyl group (see Fig. 8). According to molecular models, this leads to a core length increase of 5.9 Å. Therefore, we obtain

$$\Delta D_{\parallel}^{s}/\Delta L_c = (1.4 \pm 0.5) 10^{-4} \text{ cm}^2 \text{ s}^{-1} \text{ Å}^{-1} \quad (5)$$

in fair agreement with the above determination. From relations 3, 4, and 5, it comes immediately that

$$D_{\parallel (\text{core})}^{s} \simeq (6 \pm 1) D_{\parallel (\text{chain})}^{s} . \quad (6)$$

In that respect, the weak difference ($\simeq 5\%$) between thermal diffusivity results for PCT and PCB may look strange. However, it should be borne in mind that PCB molecules form dimers of 28 Å length,[12] i.e., close to the PCT single molecular length of 25 Å. Thus, the thermal diffusivities of both compounds have to be equivalent, as experimentally observed.

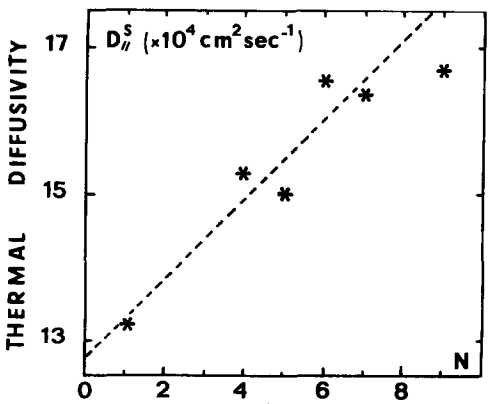

FIG. 7. Standardized (see the text) thermal diffusivity coefficient parallel to the mean direction of molecular alignment, $D_{\parallel}^{s}$, as a function of the number N of carbon atoms in the aliphatic chains. $N=1$–9 in the series of 4–4′ di (n-alkoxy) azoxy benzenes.

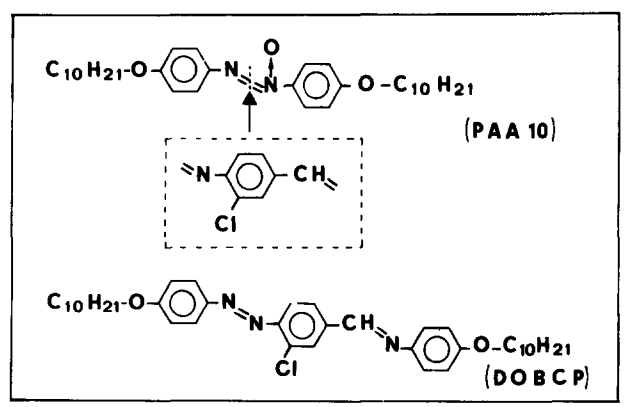

FIG. 8. Molecular structures of 4–4′-di(n-decyloxy) azoxy benzene (PAA 10 for short) and di-(4-n-decyloxybenzal)-chloro-1-4-phenylene diamine (DOBCP). Note that they only differ by the addition of one chlorosubstituted benzene group.

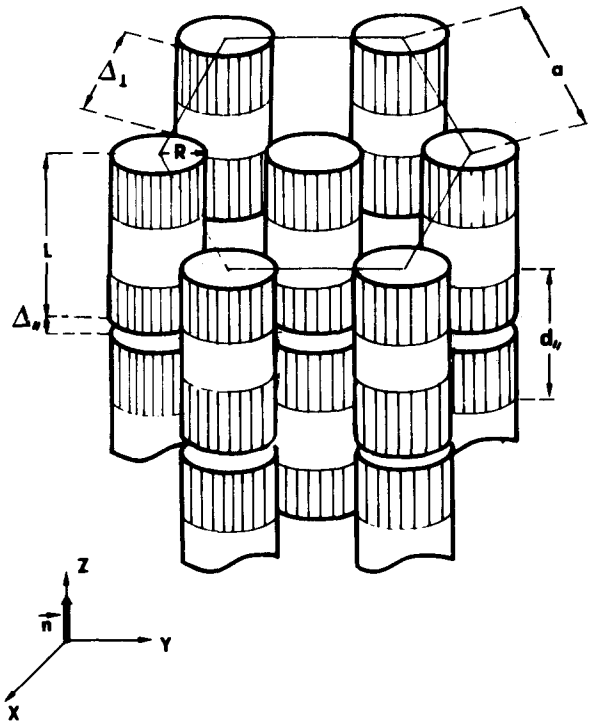

FIG. 9. Schematic representation of the molecular arrangement in a smectic B liquid crystalline phase. The hatched regions represent the low thermally conducting parts of the molecule. $\Delta_{\parallel}(\Delta_{\perp})$ is the average distance between two neighboring molecules parallel (perpendicular) to the molecular orientation axis $\mathbf{n}$. a is the lattice parameter of this hexagonal close-compact structure.

V. MODELS OF THERMAL DIFFUSION IN LIQUID CRYSTALS

Both the present experiments and our earlier results[6] support the idea that the thermal diffusivity anisotropy is closely related to the geometrical shape anisotropy of the mesogenic molecules. Increasing the length (width) leads to an increase in $D_{\parallel}^{s}$ ($D_{\perp}^{s}$). It is then tempting to make the analogy between the isolated molecule and the "box effect" observed by Biermasz and Haas in perfect solids around 5 K.[13] At these low temperatures, the mean free path of the thermal phonons is limited by the sample size and, thus, the thermal conductivity becomes dependent on the geometrical dimensions.[14] In most liquid crystalline materials, the molecules can be roughly considered as cylindrical rods of length $L \simeq 20$–40 Å. Literature data quote in the very same range the mean free path at room temperature of the phononlike modes responsible for heat conduction in liquids.[15] It is then expected that molecular dimensions will limit the phonon mean free path and consequently induce the thermal anisotropy.

We have developed this approach more quantitatively in two simple models of thermal conductivity. The first is a purely static model based on the calculation of the electrical conductance of a composite medium with regions of different conductivities. The second is an extension to anisotropic media of the Eyring thermal conductivity theory for simple liquids, and has been suggested to us by Benguigui.[16]

A. Static model

1. Electrical conductance model

A LC medium can be considered as an assembly of cylinders of radius R and length L (Fig. 9). The discontinuity of the local density at the surface of the cylinders creates a boundary resistance which strongly impedes the heat flow. It is therefore convenient to use a biphasic description. The first phase consists of the central parts of the molecules and has an infinite conductivity. The second phase is continuous throughout the specimen and consists of a thin layer of thickness Δ ($\Delta_{\parallel}$ or $\Delta_{\perp}$ depending on the direction considered) at the surface of each cylinder. Its conductivity is finite and equal to σ_0. The exact value of Δ will have to be determined experimentally. It may very well be that, in the direction parallel to the long molecular axis, $\Delta_{\parallel}$ includes a part of the flexible aliphatic chains since they are expected to have a lower conductivity than the rigid central core. This is expressed by replacing in the calculation $\Delta_{\parallel}$ by a $d_{\parallel} > \Delta_{\parallel}$. For sake of simplicity, the model has been developed for a smectic B phase, with the centers of mass of the cylinders positioned on an hexagonal compact lattice. This is justified here because, as already stated, the results do not depend on the exact nature of the mesomorphic phase, either nematic or smectic.

The computation procedure has been developed in the Appendix B. The final results write:

$$D_{\perp}^{s} = \frac{D_0}{L}[\alpha L\sqrt{3} + d_{\parallel}(1 - \alpha\sqrt{3})] \tag{7}$$

and

$$D_{\parallel}^{s} = \frac{D_0}{a^2\sqrt{3}\, d_{\parallel}}[2\pi R^2 L + d_{\parallel}(a^2\sqrt{3} - 2\pi R^2)]\,, \tag{8}$$

where D_0 is the thermal diffusivity of the homogeneous matrix, a the hexagonal lattice parameter, R the molecular radius, L the molecular length, and $d_{\parallel}$ the distance between the infinitely conducting parts of two neighboring molecules along the z axis, (see Fig. 9). α is a parameter which depends on R and a and which has been represented on Fig. 10.

2. Comparison with experimental data

Equations (7) and (8) show that the ratio $D_{\parallel}^{s}/D_{\perp}^{s}$ is independent on D_0 and can therefore be directly compared to the experimental result. On the other hand, $d_{\parallel}$ can only be obtained by solving for each compound a second order equation. Reporting that $d_{\parallel}$ value in the expression for $D_{\parallel}^{s}$ or $D_{\perp}^{s}$ allows then to calculate D_0.

The results are summarized in Table I. It is observed that $d_{\parallel}$ is nearly constant and much smaller than the molecular length L for all the compounds investigated. Its value of 1.6 ± 0.4 Å is comparable to the 1.2 Å intermolecular distance measured by x rays.[17] The fact that $d_{\parallel}$ does not vary significantly with the aliphatic chain length L_a is very surprising. It all looks

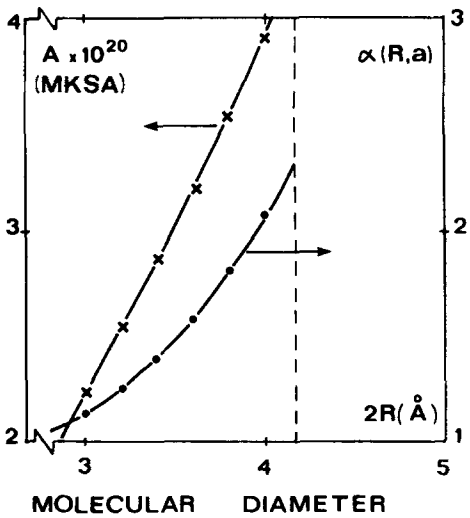

FIG. 10. Dependence of the parameters α and A, introduced in the calculations of the static model, as a function of the molecular diameter R. (see also Appendix B). The lattice parameter a is fixed at 5 Å.

as if most of the molecule was infinitely conducting with a region of finite resistance limited to a very small domain.[18] This result is in clear contradiction with our experimental observation of a widely different thermal conductivity for the aliphatic chains and the rigid molecular core respectively. Therefore, the applicability of the static model is extremely doubtful.

For the sake of completeness, we have also calculated the average thermal diffusivity of the low thermally conducting zone D_0 using Eq. (7). D_0 is found to be $(1.5 \pm 0.4) \times 10^{-4}$ cm^2 s^{-1}. This D_0 value is lower by a factor 3 or 4, than the thermal diffusivity of most organic liquids.[19] This is not unreasonable since it does not represent the bulk diffusivity, but only that of the boundary layer between the molecules.

B. Convective theory

1. Background

According to the kinetic theory arguments, the thermal diffusivity in a monoatomic gas is

$$D = \Omega_{gas} l/3 \ , \tag{9}$$

where $\Omega_{gas} = (8kT/\pi m)^{1/2}$ is the atomic velocity, m the atomic mass and l the mean free path. This expression has been later extended by Eyring to isotropic fluids by supposing that, upon molecular collision, the energy is transferred instantaneously from the center of one molecule to the center of the other.[20] On this basis

$$\Omega_{liq} = \Omega_{gas} \left(\frac{V}{V_F}\right)^{1/3} \ . \tag{10}$$

Here, V is the volume occupied per molecule and V_F the free volume. $V_F = V - v_m$, where v_m is the molecular volume (as measured from molecular models). The distance over which the energy is transported between two collisions is readily expressed as $l = V^{1/3}$. This crude argument leads to the following expression:

$$D_{liq} = \frac{l^2}{3V_F^{1/3}} \Omega_{gas} \ . \tag{11}$$

2. Application to mesophases

The Eyring expression can be easily adapted to the anisotropic, cylindrical-like, molecules of LC.[16] First, the free volume becomes anisotropic and $V_F^{1/3}$ has to be replaced by:

- $-\Delta_\parallel$ in the direction parallel to the long cylindrical axis;
- $-\Delta_\perp$ in the direction perpendicular to it.

Secondly, in order to take into account the structural complexity of the molecules, we assume that, when two molecules collide, the energy *is not* transferred instantaneously between their centers of mass. Rather, there is some part of the molecule on which the energy travels with finite speed, comparable to that of convective transfer. With this assumption, we rewrite $V_F^{1/3}$ in the following manner (Fig. 11):

$$V_F^{1/3} = \begin{cases} d_\parallel \geq \Delta_\parallel \text{ in the direction of the long cylindrical axis,} \\ d_\perp \geq \Delta_\perp \text{ in the perpendicular direction .} \end{cases}$$

For the direction parallel to the long molecular axis and since $L + \Delta_\parallel \simeq L$, Eq. (11) becomes

$$D_\parallel^s = \frac{L^2}{3d_\parallel} \Omega_{gas} \ . \tag{12}$$

Similarly, we have for the direction perpendicular to the long molecular axis:

$$D_\perp^s = \frac{a^2}{3d_\perp} \Omega_{gas} \ . \tag{13}$$

3. Comparison with experimental results

To reduce the number of unknown parameters, we first assume a fixed value of $a = 5$ Å, as suggested from

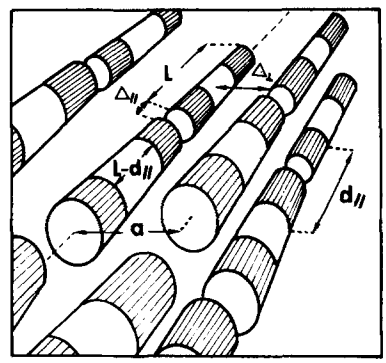

FIG. 11. Schematic representation of the molecular arrangement in a nematic liquid crystalline phase. All molecules are parallel to each other, but their centers of mass are at random. All symbols have the same signification as in Fig. 9. Note that here a corresponds to the mean distance between molecules perpendicular to their alignment axis.

the x-ray measurements.[17] Then, the $d_{\parallel}$ and $d_{\perp}$ values can be directly derived from the $D_{\parallel}^{s}$ and $D_{\perp}^{s}$ values. The results are shown in Table II. $d_{\perp}$ stays fairly constant in all investigated compounds. An average value of $d_{\perp} = 1.2 \pm 0.3$ Å is observed, which is quite comparable to the lateral displacement observed by Doucet in the smectic B phase of terephtal bis (4-n butylaniline) (TBBA).[17]

Contrary to the static model, $d_{\parallel}$ now depends on the molecular structure. For instance, $d_{\parallel}$ varies from 8 to 20 Å when going from PAA-1 to PAA-9 in the 4-4′-di-(n-alkoxy) azoxybenzenes series. This finding is clearly consistent with the observation that the aliphatic chains correspond to a region of lower thermal conductivity than the central, rigid core. We have therefore tried to relate this $d_{\parallel}$ value to the aliphatic chain length.

In Fig. 12, we have drawn $d_{\parallel}/2$ as a function of the number N of C–C bonds in one aliphatic chain [for molecules with two different chain lengths N_1 and N_2, we take $N = (N_1 + N_2)/2$]. We have also reported on the same figure the elongated chain length l_{I} in the *trans* configuration and the length l_{II} of a freely rotating chain with fixed valence angles. l_{I} has been measured from molecular models while l_{II} can be derived from the general expression proposed by Benoit[21]:

$$l_{\mathrm{II}} = \left[l_0^2 \frac{\mu(\mu^N - 1) + N(1 - \mu^2)}{(\mu - 1)^2} \right]^{1/2} + R_H \,,$$

where l_0 is the C–C length (1.54 Å), $\mu = -\cos\gamma$ with $\gamma = 109°28'$ and R_H is the van der Waals radius of the terminal methyl group.

The l_{I} and l_{II} curves are practically identical up to $N = 4$ and get progressively separated at higher values. It is immediately noticeable that our data points are better described by the l_{II}, than by the l_{I}, curve. Therefore, our thermal conductivity seems to indicate that the flexible chains adopt a conformation more akin to a freely rotating chain than to a stretched, elongated chain. This is at variance from the x-ray observation that the *trans* chain configuration is the most probable.[17]

TABLE II. Calculated values for the lengths $d_{\parallel}$ and $d_{\perp}$ of the low thermally conducting zones as derived from $D_{\parallel}^{s}$ and $D_{\perp}^{s}$, given in Table I, using Eqs. (12) and (13) of the Eyring model. L is the molecular length.

Name	L Å	$d_{\parallel}$ Å	$d_{\perp}$ Å
PAA1	19.3	8.3	1.4
PAA4	26.8	12.0	1.6
PAA5	29.3	13.8	1.3
PAA6	31.8	14.4	1.4
PAA7	34.3	16.3	1.3
PAA8	36.8	15.5	0.8
PAA9	39.3	20.5	1.1
MBBA	20.6	6.7	1.0
BBOA	30.6	13.9	1.6
CBOOA	27.8	11.5	1.2
PCB	20.3	7.1	1.0
PCT	24.9	10.8	1.4
DOBCP	49.0	17.2	0.6

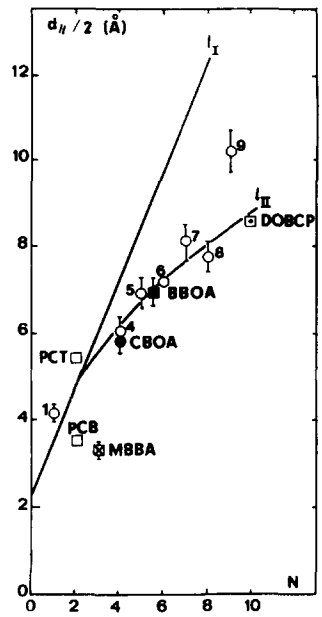

FIG. 12. Estimated lengths of the low thermally conducting molecular end parts $d_{\parallel}/2$ as a function of the number of C–C bonds in the aliphatic chains for all investigated compounds. The corresponding lengths calculated for the freely rotating chains (l_{II}) and for elongated chains in the all-*trans* configuration (l_{I}) are also given.

However, it should be realized that thermal conductivity is a rather indirect way of determining molecular conformation and should not take too much in earnest. It can also be said that, in our description, the first carbon bonds of the chain should actually be incorporated to the rigid core. This would reduce the apparent chain length contributing to the low thermal conductivity zone. Therefore, a value lower than l_{I} could indeed be expected.

At any rate, the observation of a semiquantitative agreement between our crude dynamic theory and the experimental data is already quite a satisfactory result in itself. Taking $d_{\perp} = 1.2$ Å and $d_{\parallel} = 2\,l_{\mathrm{II}}$, thermal diffusivity data of liquid crystalline materials can now be predicted to better than 20%.

VI. CONCLUSION

Using the forced Rayleigh light scattering technique, we have been able to make the first systematic study of thermal diffusivity in liquid crystals, as a function of the molecular structure:

(1) For all rodlike molecules, the diffusion is faster parallel to the long molecular axis than perpendicular to it, i.e., $D_{\parallel} > D_{\perp}$.

(2) The diffusivity values do not vary significantly from one mesophase to the other and are, thus, independent of long range order.

(3) Contrary to the other transport phenomena, there is no evidence of pretransitional effects near phase transitions between mesophases.

(4) The diffusivity anisotropy depends on the molecular shape. At fixed molecular width, it increases with molecular length.

(5) The contribution of the rigid central core to the thermal diffusivity is more important than that of the aliphatic end chains.

The first model is purely static and is based on the calculation of distributed resistances for an assembly of highly conducting cylinders embedded in a low conductivity medium. A fit to the data leads unfortunately to rather unphysical results. The length of the low thermally conducting zone is found much too small. Therefore, the different contribution to thermal conductivity of the aliphatic chains and of the rigid molecular core is not properly taken into account.

A much better agreement is obtained with our second theoretical model based on an extension to anisotropic molecules of the Eyring kinetic theory of thermal conductivity in liquids. It also assumes that the molecules are composed of one highly conducting central part and of two low conducting ends. However, a fit to the data yields estimations for the sizes of the different regions which are much more reasonable. In particular, the poorly conducting zones are found to correspond closely to the aliphatic chains. Using this model, values of the thermal diffusivities parallel and perpendicular to the long molecular axis can be obtained to within 20% for any liquid crystalline material.

To conclude, it is fair to say that the qualitative features of thermal transport in mesophases are now well understood. The next logical step would be to develop better theoretical approaches, but a frontal attack on this problem seems extremely arduous.

ACKNOWLEDGMENT

We thank L. Benguigui for pointing out the relevance of the Eyring model to the thermal transport properties of liquid crystalline materials.

APPENDIX A

Let us call **A** the tensorial quantity which relates the thermodynamic driving force **X** to the conjugated flux **J**[23]: $\mathbf{J}=\mathbf{A}\mathbf{X}$. Its principal axes will be called $\{a_i\}$ while the laboratory frame will be described by $\{x_i\}$ [Fig. 13(a)].

For uniaxial media $|\mathbf{a}_1|=a_\parallel$ and $|\mathbf{a}_2|=|\mathbf{a}_3|=a_\perp$. In the $\{a_i\}$ frame, the **X** components are

$$\mathbf{X}=\{\alpha_1 X;\alpha_2 X;\alpha_3 X\},$$

where

$$\alpha_i=\cos(\mathbf{X},\mathbf{a}_i)\ ;\quad i=1,2,3\ .$$

Therefore,

$$\mathbf{J}=\{a_\parallel\alpha_1 X;a_\perp\alpha_2 X;a_\perp\alpha_3 X\}\ .$$

1. Expression of A in the direction parallel to n

In the **X** direction, the value of **J** is

$$\mathbf{J}_\parallel=[a_\parallel\alpha_1^2+a_\perp(\alpha_2^2+\alpha_3^2)]X=A_\parallel\mathbf{X}\ .$$

Taking $\alpha_1=\cos\theta$, the expression of $A_\parallel$ becomes

$$A_\parallel(\theta)=a_\parallel\cos^2\theta+a_\perp\sin^2\theta\ .$$

2. Expression of A in the direction perpendicular to n

Consider Fig. 13(b) which is obtained from Fig. 13(a) first by a rotation of an angle ϕ around $\mathbf{x}_1$ and then by a second rotation of an angle θ around $\mathbf{a}_3$. Let **X** be parallel to $\mathbf{x}_3$ for example. With $\mathbf{a}_3$ in $x_2\,0\,x_3$ plane, one can write:

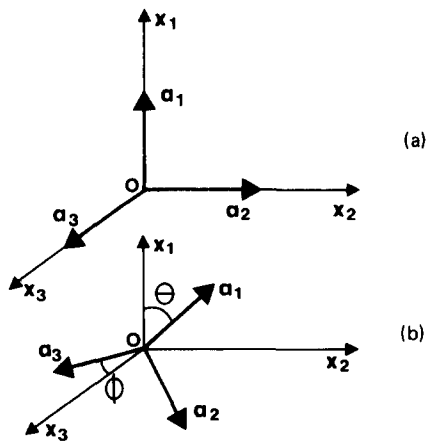

FIG. 13. (a) Referential frame used in the calculations. The $\mathbf{a}_i$ are the principal axes. The $\mathbf{X}_i$ are the laboratory frames. (b) New referential frame obtained by a rotation of ϕ around OX_1 followed by a rotation of θ around $\mathbf{a}_3$.

$$\mathbf{J}_\perp=\{a_\parallel\sin\phi\sin\theta;a_\perp\sin\phi\cos\theta,a_\perp\cos\phi\}\ .$$

Thus,

$$A_\perp(\theta,\phi)=a_\parallel\sin^2\phi\sin^2\theta+a_\perp(\sin^2\phi\cos^2\theta+\cos^2\phi)\ .$$

$A_\perp$ must be ϕ independent since the molecule is symmetrical. Taking the average value over ϕ, we get

$$A_\perp(\theta)=\frac{1}{2\pi}\int_0^{2\pi}A_\perp(\theta,\phi)d\phi\ ,$$

$$A_\perp(\theta)=\tfrac{1}{2}[a_\parallel\sin^2\theta+a_\perp(1+\cos^2\theta)]\ .$$

3. Relationship between the microscopic and macroscopic A values

The macroscopic value of **A** is obtained by performing an average around the θ position. If $f(\theta)$ is the distribution function $[(1/\pi)\int f(\theta)\sin\theta\,d\theta=1]$ the macroscopic value will be

$$\langle A\rangle=\frac{1}{\pi}\int_0^\pi A(\theta)\sin\theta\,d\theta\ .$$

Thus,

$$\langle A_\parallel\rangle=a_\parallel\langle\cos^2\theta\rangle+a_\perp\langle\sin^2\theta\rangle$$

and

$$\langle A_\perp\rangle=\tfrac{1}{2}a_\parallel\langle\sin^2\theta\rangle+a_\perp(1+\langle\cos^2\theta\rangle)\ .$$

$\langle A_\parallel\rangle$ and $\langle A_\perp\rangle$ can be expressed as a function of the order parameter $S=(3\langle\cos^2\theta\rangle-1)/2$ and we get, finally,

$$\langle A_\parallel\rangle=\frac{a_\parallel(1+2S)+2a_\perp(1-S)}{3}\ ,$$

$$\langle A_\perp\rangle=\frac{a_\perp(2+S)+a_\parallel(1-S)}{3}\ ,$$

where $a_\parallel$ and $a_\perp$ are the molecular values for $S\equiv1$ whereas $\langle A_\parallel\rangle$ and $\langle A_\perp\rangle$ are the experimental data at the temperature of measurement, i.e., for $0<S<1$.

APPENDIX B

1. Conductivity perpendicular to the long cylindrical axis

There is a formal analogy between electrokinetic and electrostatic problems when the current density **J** is replaced by the electrical field **E**. We can thus substitute the calculation of the electrical resistance R of the medium by the easier calculation of its capacitance C. Indeed it can be shown[22] that

$$R = \epsilon_0 / C\sigma_0 , \tag{B1}$$

where ϵ_0 is the dielectric permitivity of the medium and σ_0 its electrical conductivity.

We first calculate the unit cell capacity C_u shown in Fig. 14. The LC medium is then generated by connecting $(aL)^{-1}$ such cells in parallel (a^{-1} and L^{-1} in the Y and Z directions, respectively) and $(a\sqrt{3})^{-1}$ such cells in series. The total capacity per unit length is, therefore,

$$C = C_u \sqrt{3}/L . \tag{B2}$$

a. Calculation of C_u

The unit cell consist of two capacitors C_1 and C_2 associated in series. The applied electric field is parallel to **X**.

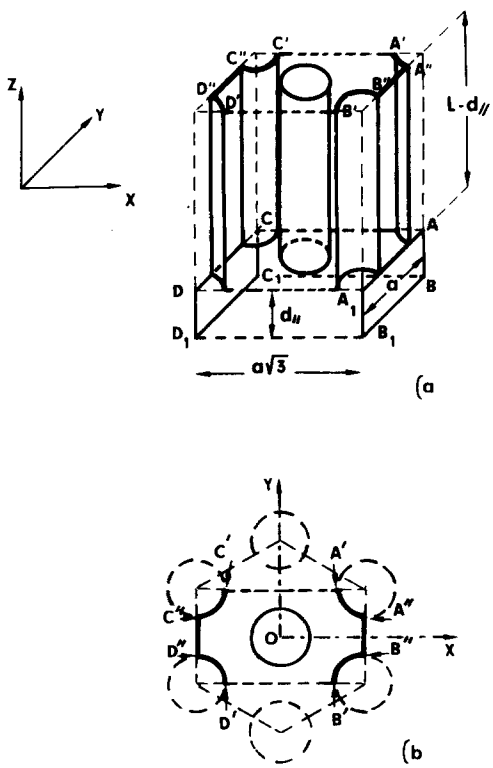

FIG. 14. (a) and (b) Schematic diagram of the unit cell used in the calculation of the capacitance. For symmetry reasons, the cylinder centered at $X_i = Y_i = Z_i = 0$ and the Y axis are at zero potential and $A'A''B''B'$ and $C'C''D''D'$ are the equipotential surfaces. These surfaces constitute the electrodes of the elementary capacitor C_1. The space between two smectic layers is represented by an additional capacity $C_2 = \epsilon_0 d_{//}/\sqrt{3}$. The total capacity of the unit cell is then $C_u = C_1 + C_2$.

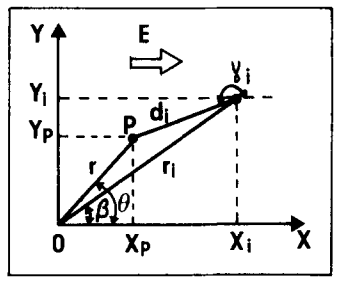

FIG. 15. Coordinates used in the calculation of the potential created by a cylinder centered at distances d_i from P and r_i from the origin.

The first capacitor C_1 has its electrodes figured by the continuous lines in Fig. 14(a). For symmetry reasons, both the supraconducting cylinder, of length $l\,L - d_{//}$ placed at the origin and the Y axis are zero potential.

The second capacitor C_2, which accounts for the poorly conducting part of the molecules and for the interspace between two neighboring molecules, has its electrodes figured by the surfaces AA_1B_1B and CC_1D_1D. These surfaces, which are separated by a distance $= a\sqrt{3}$, can be considered as equipotentials in first approximation if we neglect the end effects.

b. Calculation of C

Let us calculate the value V of the potential on the $A'A''B''B'$ surface (Fig. 14) and then derive the corresponding charge per unit length ($l = 1$) using the Gauss theorem

$$Q = \epsilon_0 \int -\mathbf{grd}\, V\, d\mathbf{S} . \tag{B3}$$

In presence of a constant electric field **E** parallel to the X axis, the problem of an equipotential cylinder centered at the origin is analogous to that of a cylindrical dipole.[24]

At any point P at a distance r from the origin, the potential $V_P(i)$ due to a cylinder placed at distances d_i from P and r_i from the origin is (Fig. 15):

$$V_P(i) = -\frac{A}{d_i}\cos\gamma_i = \frac{A}{d_i}\left[\frac{r_i \cos\beta_i - r\cos\theta}{d_i}\right]$$
$$= A[G(r_i, d_i, \beta_i)] . \tag{B4}$$

For n cylinders, in a uniform field E we obtain

$$V_P = -rE\cos\theta + A\sum_{i=-n}^{+n} G(r_i, d_i, \beta_i)$$

and in Cartesian coordinates

$$V_P = V(X_p, Y_p)$$
$$= -EX_p + A\sum_{i,j=-n}^{+n} \frac{X_i - X_p}{(X_i - X_p)^2 + (Y_i - Y_p)^2} . \tag{B5}$$

Within a smectic B layer, the cylinders are centered at points $\{X_i\, Y_i\}$. $X_i = (ia\sqrt{3})/2$ and $Y_j = a[j + (-1)^i - 1)/4]$ with $i, j \in [-n + n]$. a is the lattice parameter.

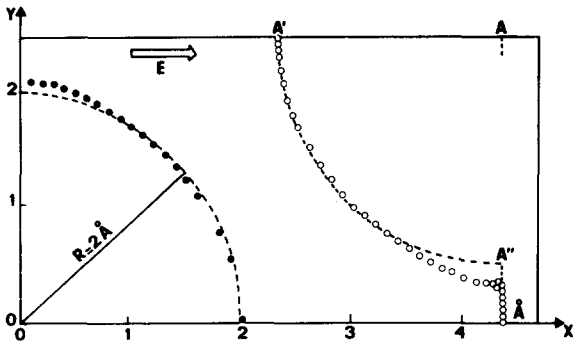

FIG. 16. Representation of two equipotential surfaces in the XOY plane of the unit cell shown in Fig. 14. The equipotential centered at the origin is obtained by setting $V_P = 0$ in Eq. (B5). For each given value of X_P ($0 < X_P < 2$) two values of Y_P were obtained. Only $Y_P > 0$ is plotted here. For the cylinder centered at $X_i = a\sqrt{3}/2$ and $Y_i = a$, we first calculated V_{P_1} at a specific point $P_1 = (a\sqrt{3}/2;\ 0)$ and then proceeds as before, but with $V_P = V_{P1}$ in Eq. (B5).

The A value is determined by the condition $V_P \equiv 0$ for $X_P = R$ and $Y_P = 0$. It is a function of R which has been calculated in Fig. 10 for R varying between 1.5 and 2.5 Å.

The numerical evaluation of the equipotentials for an assembly of ten cylinders has been performed numerically in one particular case ($R = 2$ Å and $a = 5$ Å). Figure 16 shows the equipotentials centered at $X_i = Y_i = 0$ and $X_i = a\sqrt{3}/2$, $Y_i = a/2$. They are not perfectly circular, but the deviation is less than 5% and can be neglected in first approximation. Then,

$$C_1 = \epsilon_0 l\, \alpha(R, a) , \tag{B6}$$

where α is a parameter which depends on a and R. For $R = 2$ Å and $a = 5$ Å, $\alpha = 1.507$. The variation of α vs R for a fixed value of $a = 5$ Å is presented on Fig. 10. It is observed that α increases when R increases. For R higher than 2.08 Å, the $A''B''$ part of the calculated equipotential disappears and the model proposed here is no longer valid.

c. Calculation of C_2

It is readily derived that

$$C_2 = \epsilon_0 d_{\parallel}/\sqrt{3} , \tag{B7}$$

where $d_{\parallel}$ is the distance between the two, infinitely conducting cylinders along the z axis.

d. Calculation of C_u

Summing up these two contributions, we get the capacity C_u of the unit cell

$$C_u = C_1 + C_2 = \epsilon_0 (d_{\parallel}/\sqrt{3} + \alpha l) . \tag{B8}$$

Returning to the analogy between electrostatics and electrocinetics [Eqs. (B1) and (B2)], we readily obtain the equivalent conductivity of the medium in the direction perpendicular to the cylinders

$$K_{\perp} = \frac{\sigma_0}{L}[\alpha L\sqrt{3} + d_{\parallel}(1 - \alpha\sqrt{3})] . \tag{B9}$$

2. Conductivity parallel to the long cylindrical axis

Let us first assume that the molecules belonging to successive S_B layers are perfectly in register. In each fundamental cell, the total surface of cylinders is $2\pi R^2$ and the corresponding resistance is P_1:

$$P_1 = \frac{d_{\parallel}}{\sigma_0 2\pi R^2} . \tag{B10}$$

The remaining part of the cell have a resistance P_2

$$P_2 = \frac{L}{\sigma_0(a^2\sqrt{3} - 2\pi R^2)} . \tag{B11}$$

The total unit cell resistance is obtained by adding these two resistances in parallel

$$P_F^{-1} = P_1^{-1} + P_2^{-1} . \tag{B12}$$

Since there are L^{-1} such resistances associated in series and $(a^2\sqrt{3})^{-1}$ in parallel, the total resistance per unit length of the medium P_T writes:

$$P_T = \frac{a^2\sqrt{3}}{L} P_F . \tag{B13}$$

The corresponding conductivity is

$$K_{\parallel} = \frac{\sigma_0}{a^2 d_{\parallel}\sqrt{3}}[2\pi R^2 L + d_{\parallel}(a^2\sqrt{3} - 2\pi R^2)] . \tag{B14}$$

3. Final expressions for the thermal diffusivities

The analytical expressions for $D_{\parallel}$ and $D_{\perp}$ can be easily derived from the Eqs. (B9) and (B14) for $K_{\parallel}$ and $K_{\perp}$ using the well-known relationship $D = K/\rho C_p$, where ρ is the specific gravity and C_p the thermal capacity.

[1] E. Guyon, P. Pieranski, and F. Brochard, C. R. Acad. Sci. Ser. B **273**, 486 (1971); R. Vilanove, E. Guyon, C. Mitescu, and P. Pieranski, J. Phys. (Paris) **35**, 153 (1974).

[2] C. K. Yun, J. Appl. Phys. **42**, 4764 (1971); M. Longley-Cook, Ph. D. Thesis, University of Arizona, 1972.

[3] H. Eichler, G. Salje, and M. Stahl, J. Appl. Phys. **44**, 687 (1969).

[4] In principle, thermal conductivity can also be obtained from the attenuation of sound propagation. However, it has been shown that, in liquid crystals, the major contribution to attenuation is due to viscous terms. The attenuation due to the thermal conduction has been calculated to be four orders of magnitude smaller, K. Miyano and J. B. Ketterson, *Physical Acoustics* (Academic, New York, 1979), Vol. 14, p. 93.

[5] D. W. Pohl, S. E. Schwarz, and V. Irniger, Phys. Rev. Lett. **31**, 32 (1973).

[6] (a) W. Urbach, H. Hervet, and F. Rondelez, Mol. Cryst. Liq. Cryst. **46**, 209 (1978); (b) F. Rondelez, W. Urbach, and H. Hervet, Phys. Rev. Lett. **41**, 1058 (1978).

[7] P. G. de Gennes, *The Physics of Liquid Crystals* (Clarendon, Oxford, 1975).

[8] H. Hervet, W. Urbach, and F. Rondelez, J. Chem. Phys. **68**, 2725 (1978).

[9] W. Urbach, Ph. D. thesis, Université Paris-Sud, Centre d'Orsay, France (1981).

[10] W. Urbach, M. Boix, and E. Guyon, Appl. Phys. Lett. **25**, 479 (1974).

[11] F. Hardouin, M. F. Achard, and F. Gasparoux, Solid State Commun. **14**, 453 (1974).

[12] P. E. Gladis, R. K. Bogardus, and D. Adsen, Phys. Rev. A **18**, 2292 (1978).

[13]W. J. de Haas and T. Biermasz, Physica **2**, 673 (1935); **4**, 752 (1937); **5**, 47, 320, 619 (1938); see also R. Berman, Proc. R. Soc. London Ser. A **208**, 90 (1951).
[14]H. B. G. Casimir, Physica **5**, 495 (1938).
[15]P. A. Egelstaff, *An Introduction to the Liquid State* (Academic, New York, 1967).
[16]L. Benguigui (private communication).
[17]J. Doucet and A. M. Levelut, J. Phys. (Paris) **38**, 1163 (1977); see also, J. Doucet, Ph.D. thesis, Universitè Paris-sud, Centre d'Orsay, France, 1978.
[18]Note that if, according to the relationship given in Eq. (6), a finite core conductivity is injected in the model, the $d_{\parallel}$ value would be even lower.
[19]*Handbook of Chemistry and Physics*, edited by R. C. Weast (Chemical Rubber, Cleveland, Ohio).
[20]J. O. Hirschfelder, C. F. Curtis, and R. B. Bird, *Molecular Theory of Gases and Liquids* (Wiley, New York, 1954), p. 633.
[21]M. H. Benoit, J. Chem. Phys. **44**, 18 (1974).
[22]Y. Rocard, *Electricité* (Masson, Paris, 1956), p. 154.
[23]We neglect the off-diagonal terms $a_{ij}(a_{ii} \gg a_{ij})$ since we only consider here uncoupled transport processes.
[24]By cylindrical dipole, we mean two parallel wires running in the Z direction and with equal and opposite linear charge densities.